# A Synergy-Based Control Solution for Overactuated Characters: Application to Throwing

Ana Lucia Cruz Ruiz, Charles Pontonnier, Jonathan Levy, Georges Dumont

# A Synergy-Based Control Solution for Overactuated Characters: Application to Throwing

Ana Lucia Cruz Ruiz

INRIA/IRISA

École Normale Supérieure de Rennes, Bruz, France

Campus de Beaulieu

263 Avenue Général Leclerc

35042 Rennes,France

Tel. (+33)299847413

email: ana-lucia.cruz-ruiz@inria.fr

Charles Pontonnier

Écoles de Saint-Cyr Coëtquidan, Guer, France

IRISA/INRIA, Rennes, France

École Normale Supérieure de Rennes, Bruz, France

Jonathan Levy

École Normale Supérieure de Rennes, Bruz, France

Georges Dumont

École Normale Supérieure de Rennes, Bruz, France

IRISA/INRIA, Rennes, France

**Abstract**

In the current paper, we present a bio-inspired solution for the control of overactuated models in animation, such as musculoskeletal models. This solution consists in the extraction of muscle synergies from human experiments, followed by a control method consisting of a series of optimizations to adapt muscle parameters and synergies to match experimental data. We apply the framework on throwing motions and the results show that these motions can be accurately reproduced on a character with a simplified muscular structure, while preserving important characteristics in the original synergies or control signals.

**Keywords:** motion synthesis, physics-based animation, optimization, musculoskeletal model, muscles

# Introduction

Historically, physically-based character motion synthesis has been dominated by torque-based animations [1, 3, 4], that is, the use of characters actuated by ideal servo motors. However, this field is currently reaching a tipping point with the introduction of muscle-based animation, or animations in which characters are actuated by muscle models [2]. The beneficial level of actuation abstraction for specific applications is yet to be defined, and more exhaustive studies comparing muscle-based and torque-based animations are needed to evaluate their benefits and setbacks. Nevertheless, the benefits of muscle-based animation have begun to inspire animators, resulting in partially or entirely muscle-based characters.

Studies from the fields of biomechanics and animation are showing the importance of focusing on a more accurate actuation modeling instead of trying to compensate this lack of realism with a complex control law. They have evidenced that the presence of viscoelastic and non-linear actuators [6], result in: 1) better energy estimates for optimization-based controllers [7, 8], 2) characters with better stability properties and more realistic passive dynamics [9, 10, 11, 12], 3) a mechanical system with the ability to perform control functions by itself [13, 14, 15], and 4) an ease to simulate musculoskeletal defects, pathologies and fatigue [7, 16, 8].

However, using muscle as actuators in animation also implies solving important challenges [2], such as: redundancy, non-linearity, and underactuation. First of all, muscle-based characters are redundant or overactuated, meaning that they have more actuators than

degrees of freedom (Dofs). This redundancy complicates the resolution of the forward dynamics problem because an infinity of muscle forces achieve the same motion [17]. Second, muscles are non-linear visco-elastic actuators [6], meaning that their control is not straightforward and needs to be formulated through sophisticated non-linear control theories to properly achieved the desired motion [18]. Finally, muscles can also lead to underactuation, since a single muscle can actuate several degrees of freedom simultaneously with different degrees of contribution. In this work we will mainly focus on the first challenge: the redundancy and overactuation of muscle-based characters.

State of the art approaches have dealt with this overactuation through optimization-based controllers that are able to compute a high number of muscle control signals, but are complex, and are not likely to represent the intuitive mechanisms behind human motion generation. These controllers have been recently classified as either: controller optimization methods or trajectory optimization methods [2] . Controller optimization methods seek to optimize the parameters of a specific control law in order to produce muscle signals that satisfy specific motion goals, while trajectory optimization methods directly generate the muscle trajectories that accomplish the desired motion goals.

Some examples of controller optimization methods include the optimization of PD controllers and muscle reflex laws to synthesize walking and running motions [8, 21], and of PD controllers and neural networks to synthesize swimming motions [22]. Examples of trajectory optimization methods include, encoding control trajecories as splines and using trajectory optimization and spacetime constraints to synthesize walking and kicking motions

[23], and adapting muscles to simulate gaits with conditions such as muscle weakness, joint dislocation, tightness, pain reduction and maximization of efficiency [16] .

The previous control strategies are able compute a large number of muscle control signals to achieve a specified goal, but they do not question the hypothetical link (or synergy) between them. The existence of such a link is an active research area in neuroscience, and would help reducing the complexity of the problem since a lower number of control signals would have to be determined. Some authors have already exploited this idea in kinematic and torque-based animations, either to identify low dimensional control representations [24], or to identify the Dofs that have higher contributions to the motion and that need be controlled via a primary control strategy [25, 27].

The purpose of this study is to propose a synergy-based solution for muscle-based characters. A compact solution that exploits the hypothetical link between muscle control signals to address one of the main challenges of muscle-based animation: redundancy. Through the use of synergies, our solution allows muscles to be controlled in groups and not individually. In the following sections, we will explain what synergies are, how they can be extracted from human data, and finally how they can be used as a simple control representation for commanding muscle-based characters during an overhead throwing motion example. A motion that is highly redundant, and that requires higher coordination, accuracy, and skill than simple manipulation tasks. The framework has been partially previously presented [20], however we extend its capabilities by reducing control redundancy further, and better preserving the original human recorded synergies.

# Material and Methods

## Time-invariant synergy definition

Muscle synergies are defined as patterns of coordinated activations applied to a group of muscles [28, 29]. The muscle synergy hypothesis assumes that the central nervous system (CNS) translates task level commands into a reduced number of modules or synergies, which are later mapped into a larger set of individual muscle activations [19, 30]. Since synergies are less numerous than the number of muscles, they can be used to create compact and reduced control representations.

Time-invariant or synchronous muscle synergies are one of the ways neuroscientists represent synergies. This model was chosen as the basis to our synergy-based control solution. Mathematically, a synchronous synergy $w_i$ is defined as a D-dimensional vector of coefficients, specifying the relative activation level of D-muscles. Each synergy is paired with a time-varying combination coefficient vector $c_i(t)$, which determines its temporal evolution. A set of N-synergies can be linearly combined to generate D-muscle activation patterns $A(t)$:

$$A(t) = WC(t) = \sum_{i=1}^{N} w_i c_i(t) \tag{1}$$

Where, $A(t)$ is the $D \times T$ samples matrix containing the recorded muscle activations patterns, $W$ is the $D \times N$ muscle synergy matrix, and $C(t)$ is the $N \times T$ samples combination

coefficient matrix.

## Data collection and synergy extraction

The protocol used for data collection and synergy extraction has been partially previously presented [31]. Data was collected from overhead football throws to 2m, 4m and 7m targets (a description of this motion is featured in Figure 1). During this action, body kinematics and muscle activation patterns were collected from a healthy 32-year old male (stature 1.86m, weight 72 kg). The activity of 6 right arm muscles was recorded: the deltoid posterior and anterior, the biceps, the triceps long, and the wrist extensors and flexors, which were recorded as a group. These muscles were chosen due to the correspondence of their roles, with the roles of the muscles in our character (section *Character model*). The details on the equipment used and data processing is detailed in Appendix A.

Once the EMG signals are processed different matrix factorization algorithms can be used to extract the synergies [35]. We opted for a NMF (Non-negative matrix factorization) algorithm [36]. NMF has a robust performance in a large extent due to the strong constraints imposed by its assumption of nonnegativity. This algorithm was used to extract a set of synchronous muscle synergies (section *Synergy extraction results*) and their corresponding combination coefficients from the recorded EMG pattern matrix $A(t)$. A matrix, which was constructed by concatenating the EMG data of 18 throws or 6 throws per throwing distance.

Essentially, NMF decomposes a non-negative matrix into a non-negative linear combi-

nation of basis vectors, by solving the following optimization problem:

$$\begin{aligned} \underset{W,C}{\text{minimize}} \quad & \frac{1}{2}||A(t) - WC(t)||_F^2 \\ \text{subject to} \quad & W, C(t) \geq 0 \end{aligned} \tag{2}$$

In this extraction, actuation redundancy was minimized by choosing the number of synergies ($N = 2$) to be less than the number of degrees of freedom ($ndofs = 3$) and muscles ($D = 6$) in the model described in the next section. Moreover, the extraction was made from the recorded activations of $6$ muscles of the arm which have matching actions with the muscles in our model. The extracted synergies and their time-varying combination coefficients are presented in section *Synergy extraction results*.

## Character model

The character used in this study was developed in MATLAB® SimMechanics. It consists of a full body skeletal model with a musculoskeletal arm (Figure 2). The skeletal model consists of $21$ rigid bodies linked by $17$ joints, and exhibits $32$ degrees of freedom (Appendix B). The right arm of the skeleton is actuated by six muscles (with actions on the sagittal plane) which are known to have important contributions in the task of throwing. The following sections detail further the musculoskeletal arm model and its actuation.

**Musculoskeletal arm model**

The arm exhibits 3 degrees of freedom at the shoulder, 2 at the elbow and 2 at the wrist. The muscle-actuated degrees of freedom are the shoulder, elbow and wrist flexion (positive motion) and extension (negative motion). The remaining degrees of freedom of the arm are kinematically driven.

For simplicity, pairs of antagonistic muscle models were used in order to reflect the action of real muscles on the segments [45] . Figure 2 features a view of the musculoskeletal arm from the sagittal plane. The first antagonistic pair ($m_1$ and $m_2$) simulates the actions of the deltoid anterior and posterior on the shoulder. Therefore, the contraction of muscle $m_1$, produces shoulder flexion, while the contraction of muscle $m_2$ produces shoulder extension. The second pair ($m_3$ and $m_4$) simulates the actions of the biceps and triceps long on the elbow, flexing and extending the elbow. And finally the third pair ($m_5$ and $m_6$) simulates the actions of the wrist flexor and extensor group. The effect and interactions of these muscles with the skeleton can be characterized geometrically and functionally.

Figure 3 features the geometry of a single musculotendon unit, and an example of a changes in length during an elbow extension. Each musculotendon unit is composed of a muscle and an infinitely rigid tendon of constant length. The muscle routing is pulley-like. In other words each unit is wrapped around a circumference of constant radius $r_{j,k}$, centered at the axis of rotation of its corresponding degree of freedom $q_k$. The changes in length of these units are given with respect to a joint rest position $qr_k$ and a musculotendon rest length

$l_{mtr,j}$. The total length of the musculotendon unit can be mathematically expressed as:

$$l_{mt,j} = l_{mtr,j} - r_{j,k}(q_k - qr_k) \tag{3}$$

Where the musculotendon resting length $l_{mtr,j}$ is simply the sum of the muscle rest length $l_{mr,j}$ and constant tendon length $l_{t,j}$:

$$l_{mtr,j} = l_{mr,j} + l_{t,j} \tag{4}$$

Each musculotendon unit can apply a force $F_{m,j}$ on a specific degree of freedom, generating a torque that moves the skeletal system. Therefore, the total torque of a set $D_k$ of muscles on the degree of freedom $k$ can be expressed as:

$$\Gamma_k = F_{m,j}(a_j, F_{o,j}, l_{mt,j}, \dot{l_{mt,j}}) \cdot r_{j,k}, \quad j \in D_k \tag{5}$$

Where $F_{m,j}$ is a function of the muscle activation signal $a_j$, the maximum isometric force $F_{o,j}$, and musculotendon unit's length $l_{mt,j}$ and shortening velocity $\dot{l_{mt,j}}$. The functional Hill muscle model was used to compute the muscle force [6]. Details on this model, the force computation, and muscle geometry can be found in Appendix B.

Finally, complete dynamics of the musculotendon unit also includes the activation dynamics, which describes the non-linear temporal relationship between the neural excitation and the effective activation of the muscle [46]. This non-linear relationship can be approximated by a second order differential equation [47, 48], exhibiting different time constants

for activation and deactivation:

$$\dot{e}_j = (u_j - e_j)/\tau_{ne}$$

$$\dot{a}_j = \begin{cases} (e_j - a_j)/\tau_{act} & , \quad e_j \geq a_j \\ \\ (e_j - a_j)/\tau_{deact} & , \quad e_j < a_j \end{cases} \tag{6}$$

Where $u_j$ is the neural excitation, $a_j$ the muscle activation, $e_j$ an intermediate variable, $\tau_{ne}$ the neural excitation time constant (often neglected), $\tau_{act}$ and $\tau_{deact}$ the activation and deactivation time constants respectively. In the current work, activation dynamics was taken into account a posteriori as it is shown in section $C(t)$ *optimization and filtering*.

## Synergy-driven forward dynamics pipeline

The character model was used within the synergy-driven forward dynamics pipeline in Figure 4. The aim of this pipeline is to replay the recorded human arm motion $q^d$ on a virtual arm by using muscle synergies. Essentially, the pipeline tries to overcome two limitations that prevent a perfect motion reconstruction using the raw synergies: the uncertainty in muscle parameters, and the distinct dynamics of the character model with respect to the real human. This is achieved through two consecutive adaptation stages: a muscle parameter ($P$) optimization, and a synergy combination coefficient ($C(t)$) optimization and filtering. At each iteration the output of these procedures is used in the conversion from muscles syn-

ergies to muscle activations $A(t)$, which finally results in skeletal motion that is used in the evaluation of the optimizations.

In the first optimization stage (the muscle parameter optimization), the unknown muscle parameters of the character are determined, and we evaluate if the original recorded synergies encode essential information that allow general trends in the motion to be reproduced. In the second optimization stage ($C(t)$ optimization and filtering), we adapt the original synergies to our character's distinct dynamics in order to reproduce the desired motion.

## Muscle parameter optimization

Muscle parameters are subject specific and are initially unknown. The estimation of such parameters is important since they affect the mapping from synergies to motion. Therefore, an optimization was designed in order to determine a set of parameters that enhanced this mapping. These parameters were: the maximal forces $F_{o,j}$, moment arms $r_{j,k}$, rest lengths $l_{mr,j}$, and joint rest positions $qr_k$. The following optimization was repeated for each muscle-actuated degree of freedom $q_k$ with the purpose of finding the parameters $P_k$ of the muscles acting directly on it:

$$\begin{aligned} &\underset{P_k}{\text{minimize}} \quad \sum_{h=1}^{Nsamples} (q_k(t_h) - q_k^d(t_h))^2 \\ &P_k = [F_{o,j}, l_{mr,j}, r_{j,k}, qr_k], \quad j \in D_k, \quad P_k \in P \end{aligned} \tag{7}$$

$$\text{subject to} = \begin{cases} F_{o,j} > 0 \\ r_{j,k} > 0 \text{ or } r_{j,k} < 0 \text{ (action dependent)} \\ 0.8 \leq \frac{l_{mr,j}}{lo,j} \leq 1.2 \\ -180^{\circ} \leq qr_k \leq 180^{\circ} \end{cases}$$

Where, $Nsamples$ is the total number of samples, $t_h$ is the current time sample, $D_k$ is a set containing the muscles acting on joint $q_k$, and $P$ is the set containing the parameters for all joints. The constraints on $r_{j,k}$ are action dependent. In other words the moment arms are positive or negative depending on the sign of their expected actions on the joints. The constraints on $l_{mr,j}$ correspond to known intervals for this value with regard to $l_{o,j}$, the optimal fiber length or the length at which the muscle has its greatest ability to produce force.

Average initial values for $F_{o,j}$ and $r_{j,k}$ were based on biomechanical studies [40], and each muscle was assigned values based on the real muscle it simulated (section *Musculoskeletal arm model*). For the wrist extensor and flexor group, the parameters of the extensor carpi ulnaris and flexor carpi radialis were used. However, certain parameters, such as $qr_k$ and $l_{mr,j}$, had to be arbitrarily chosen since they are specific to the muscle model used.

This, and following optimization problems were solved in MATLAB® via the *fmincon* function and its *interior-point algorithm*. In each optimization, only the degree of freedom of interest was populated with muscles, while the rest of the skeleton was driven kinemati-

cally. At each iteration, the entire throw was simulated by driving the arm with the extracted synergies. Then, the global error on joint position was computed, and new muscle parameters were proposed for subsequent iterations until the error was minimized.

## $C(t)$ optimization and filtering

The character model will always be a rough approximation of the real recorded human (with different mass, muscle parameters, muscle routing etc.) Therefore, a part of the control signals (synergies) should be adapted to deal with the distinct dynamics of the model. To address this, while the task independent part of the synergies, synergy matrix $W$, was kept unmodified, an optimization was implemented to adapt the task dependent part of the synergies, or time-varying combination coefficients $C(t)$, at each time step:

$$\begin{aligned} &\underset{c_i(t_{h-1})}{\text{minimize}} \quad \sum_{k=1}^{ndofs} |q_k(t_h) - q_k^d(t_h)| \\ &\text{subject to} \quad 0 < c_i(t_{h-1}) < 1, \\ &c_i(t_{h-1}) \in C(t_{h-1}), \quad i = 1...N \end{aligned} \tag{8}$$

Where $ndofs$ is the total number of muscle actuated degrees of freedom in the model (3 in our case), and $N$ is the number of synergies.

The previous optimization routine did not take into account the muscle activation dynamics and often resulted in a apparently noisy signal. In fact, after optimization, the resulting signal was more comparable to a neural excitation than to a real muscular activation due to the lack of dynamical evolution in the muscle model used. We circumvented this issue by

applying a second order numerical filter to the optimized signal, representing the activation dynamics, thanks to the model presented in section *Musculoskeletal arm model*.

Assuming that the activation and deactivation constant times are equal, and that the relation between $C(t)$ and the activation $A(t)$ is straightforward, equation 6 can be written in the Laplace domain as:

$$\frac{c_i(p)}{c_{iraw}(p)} = \frac{1}{(1+\tau_{act}p)(1+\tau_{ne}p)} \tag{9}$$

Where $c_{iraw}(p)$ represents the optimized coefficients before filtering and $c_i(p)$ represents the coefficients after filtering. The time delays, $\tau_{act}$ and $\tau_{ne}$, were set to $50$ms and $1$ms respectively. For more details on the implementation of this filter the reader is invited to consult the Appendix C.

# Results and Discussion

## Synergy extraction results

Through the application of the synergy extraction algorithm described in section *Data collection and synergy extraction*, a 2-synergy model was obtained. Figure 5 features the synergies $w_i$ in this model, which capture the relative activation levels of the muscles throughout the entire motion. Figure 6 depicts the combination coefficients $c_i$ which encode when and with what intensity each synergy is triggered for all the concatenated throws. The shape of these coefficients is repeatable across throws, with only small differences in amplitude and

time duration.

Each synergy recruits groups of muscles with biomechanical actions corresponding to specific motion phases [31]. For instance, in this synergy model we can see how the muscle activations were grouped into an agonist and an antagonist synergy. As seen in Figure 5, the first synergy (agonist) contains a high activation of muscles corresponding to shoulder flexion, internal rotation (deltoid anterior), and elbow extension (triceps long). While the second synergy (antagonist) contains a higher activation of muscles corresponding to shoulder extension, external rotation (deltoid posterior), and elbow flexion (biceps).

First, the antagonist synergy is triggered in the beginning of the motion. Next, its activation is diminished until the agonist synergy is triggered towards the end of the acceleration phase when the ball is released. At this point the antagonist synergy is triggered again, and a considerable amount of synergy co-activation occurs. This is consistent with the fact that ballistic movements exhibit concurrent agonist and antagonist muscle activation [49]. During these motions, a first activation is needed to accelerate the limb towards the target (agonist), followed by a second activation to decelerate and stop the movement (antagonist). This sequence of bursts (from antagonist to agonist, and from agonist to antagonist) are characteristic of the antagonist activity in the upper extremity while throwing. Such "triad" burst sequences have already been identified in EMG analysis of throwing (at the wrist and elbow muscles) [50], and in badminton smash strokes [51]. Furthermore, the increment in the amplitudes of the combination coefficients as the throwing distance increases, is consistent with the increment in torque magnitudes observed during the synthesis of throwing

motions to different ranges [52].

In the next sections we present the results of using these synergies in our synergy-driven forward dynamics pipeline. Since the synergy model was created by concatenating several throws together, we used the section of the $c_i$ signals corresponding to a single 2m throw.

## Synergy-driven motion with uncertain muscle parameters

The synergies were first used to drive the $6$ muscles in the character ($m_1$ to $m_6$) with uncertain parameters and without the synergy adaptation procedure. Figure 7 features the resulting angular trajectories versus the trajectories obtained from motion capture data for the $3$ muscle-driven degrees of freedom.

As expected, the motion did not follow the general trends of the desired joint trajectories. Only in the beginning of the motion the reconstructed and original trajectories are similar. The expected behaviors (shoulder flexion, elbow extension, and wrist extension) begin to develop but turn into high oscillations and diverge from the desired positions.

It is important to highlight that this behavior is bound to happen, since we are using a very simple representation of the real human from which the synergies were extracted, especially in terms of muscle routing. Moreover, the mapping made from synergies to motion was hindered by the arbitrary choice of resting angles and lengths. These parameters are unknown and they determine the equilibrium position of the joint.

## Synergy-driven motion with optimized muscle parameters

As seen in the previous section, the use of arbitrary muscle parameters has a large impact on the mapping done from activations to kinematics. Thus, the adaptation stage described in section *Muscle parameter optimization* was applied in order to determine a set of muscle parameters that enhanced this mapping. The application of the synergies using the optimized parameters resulted in the motion featured in Figure 8. Compared to the previous section, we can see a significant improvement in the resulting kinematics since most muscle-driven joint trajectories follow quite correctly the recorded ones.

The quality of the reconstructed kinematics can be evidenced via the coefficient of determination for each degree of freedom, which were $r^2_{shoulder} = 0.8939$, $r^2_{elbow} = 0.8843$, and $r^2_{wrist} = 0.2732$. Compared to our previous work [20], these coefficients were maintained (Table 1). This evidences that a very similar motion reconstruction can be obtained with a lower dimensional synergy model, and that this representation encodes essential muscle activation information.

The reconstructed kinematics show that the synergies are able to capture and roughly reproduce general trends in the joint positions. These trends can be seen by analyzing each degree of freedom closely. For example, shoulder flexion gradually increases and then decreases towards the end of the motion. Elbow extension is made halfway through the motion (during the acceleration phase) as the highest wrist extended position is reached.

However, minor oscillations are presented in the reconstructed motion and a consider-

able delay is seen for the wrist trajectory. This behavior can be a consequence of the fact that all muscle parameters were not optimized in one sole procedure.

## Optimized synergy-driven motion

Next, it was necessary to modulate when and how much each synergy $w_i(t)$ was triggered according to the character model and the desired positions. Therefore, the next adaptation stage consisted in optimizing and filtering the time-varying combination coefficients as described in section $C(t)$ *optimization and filtering*. The reconstructed and recorded kinematics are featured in Figure 9, while coefficients before and after the optimization and filtering are featured in Figure 10.

The resulting motion follows more closely the desired kinematics. The coefficient of determination for all degrees of freedom was improved, especially for the wrist ($r^2_{shoulder} = 0.8859, r^2_{elbow} = 0.9489, r^2_{wrist} = 0.6746$). Once again, the quality of reconstruction was comparable to that of our previous results [20] (Table 2), with a slight decrease in the wrist coefficient of determination, and an increase in the elbow. Animated versions of the synergy-driven motions are featured in the accompanying video [1].

The results validate the control strategy we adopted as a relevant direct dynamics motion control strategy. They also prove the significance of our initial synergy estimation, since the synergy coefficient shapes were well preserved after the optimization and filtering (Figure 10). For instance, although the antagonist synergy was significantly modified, we can see

[1] Online version: https://youtu.be/PMrjToIKfYM

that the triggering times and intensity of the agonist synergy reflect well those of the initial synergy.

Furthermore, by computing the cross-correlation between the recorded and optimized coefficients (Figures 11 and 12), we can see that our current model is better preserved than our previous one after the optimization and filtering [20]. Our previous 5-synergy model is characterized by wider spreading of high correlation peaks, sometimes at considerable lags [20] . However, the agonist synergy of our 2-synergy model is characterized by a bell-shaped curve with a maximum correlation at almost zero lag.

Nevertheless, clear differences can also been seen between the initial and optimized coefficients of our current synergy model, specially for the antagonist synergy. The causes of these differences stem from a set of limitations that will be discussed in the following section.

## Limitations and perspectives

The control solution presented in this paper significantly reduced actuation redundancy, while maintaining a good motion reconstruction quality and preserving important characteristics in the original control signals (or synergies). The preservation of these synergies was due to the fact that we removed unnecessary information from our previous synergy model [20], by making an extraction from the relevant muscles only. However, if the framework is to be extended to more degrees of freedom in the future, then a larger set of muscles would

be used for the extraction.

The pipeline also has limitations that still need to be resolved. The first limitation is linked to the simple muscle models used. The current muscle routing assumes constant moment arms to each degree of freedom, which comes at a cost. The resulting motion is distorted and this causes a need for unnecessary adaptations of $C(t)$. A more realistic muscle routing could be achieved by including time-varying moment arms, which will vary the capacity of the muscle to exert torque against the joint positions. Another important modeling aspect that was not considered a priori was the activation dynamics. This relationship between excitations and activations has a natural filtering effect, which will lead to smoother motions.

Another limitation is the fact that a unique muscle parameter optimization was not made. Instead, individual optimizations were made on each degree of freedom. This has the effect that muscle parameters corresponding to each degree of freedom are optimized under different dynamic conditions, by assuming a perfect motion for the remaining degrees of freedom. Thus, when driving the three degrees of freedom of interest with synergies and optimized muscle parameters the overall motion reconstruction quality is hindered. By driving the degrees of freedom of interest simultaneously with synergies and performing one sole parameter optimization, a higher motion reconstruction quality is expected. Furthermore, the muscle parameter optimization itself could benefit from the use of global search methods that guarantee the discovery of a better set of parameters in a shorter period of time.

Lastly, another limitation is the high computation time. An issue that is shared among

approaches which involve the control of musculoskeletal models. Some state of the art approaches can need from 10h to 12h and/or several computer cores to synthesize some seconds of animation [8, 21, 16]. Our framework is also computationally expensive. Initially in our previous work, the total parameter optimization time was of 1h and the synergy coefficient optimization was of 12h on an HP Intel(R) Core(TM) i7-3740QM CPU 2.70GHz [20]. Since the number of control variables was reduced from 5 to 2, currently the synergy optimization has been reduced from 12h to 8h. Nevertheless, the pipeline used in the current paper is not optimized at this point and computation time may be certainly improved.

We believe that by addressing the limitations described above even less modifications will be necessary on the synergy combination coefficients. Additionally, these coefficients could be optimized using procedures that better preserve their shapes, such as a dynamical optimization.

Our future work will include three further enhancements: 1) the formulation of relationships between task space goals and the variations in the combination coefficients $C(t)$ (both raw and optimized), 2) the synthesis of new motions by specifying task-space goals (ball release height, velocity, and angle) and synergy adaptation, and 3) the extension of the framework for the control of a higher number of degrees of freedom.

The framework also has the potential to be extended to other motions by creating a richer database of synergies with respect to standard task-space goals. Such a database could be based on other arm motions such as writing, pointing, and other arm gestures.

Finally, it is worth noting that the notion of synergies can be used to reduce the com-

plexity of a control problem either at the kinematic or actuation level (torque or muscular level). The disadvantage of using synergies in a muscular space over the other levels, is that a stronger reduction is needed (since there are more muscles than Dofs). Thus, the synergies should encode a larger quantity of information, which can lead to a higher loss of information at low order synergy models. Nevertheless, a key advantage of using synergies in a muscular space is that a separation can be made between the agonist and antagonist actions on each DoF and that these can be controlled in different groups. Such representation resembles more closely the grouping of agonist and antagonist actions of real muscles on humans.

# Conclusion

Physics-based character motion synthesis is a growing field in animation. With evidence highlighting the benefits that realistic actuation modelling has on the final motion, there is a need to implement control strategies that handle new challenges. One of these challenges is the higher redundancy of muscle-based characters with regard to torque-driven simulations. State of the art approaches have produced outstanding results, but have chosen to handle this redundancy via heavy optimizations that compute a large number of control signals (usually one per muscle) [2, 21, 8, 16].

A more realistic and intuitive solution should control the motion as whole by establishing relationships between the different actuators and coordinating them as a group to achieve

the final task. The goal of this work was to identify these links in order to create a compact control model (synergy model) able to reproduce a motion on a virtual character, while also reducing redundancy.

We first introduced the concept of muscle synergies and the experimental protocol used to identify them. Next, the musculoskeletal model and forward dynamics pipeline were presented. Results showed that: 1) 2 synergies encode the essential information needed to control a 3-Dof virtual arm with 6 muscles, (2) the raw extracted synergies are able to reproduce important kinematic trends on a simple virtual arm, and (3) motion reproduction can be enhanced by modifying the synergy coefficients, while also preserving important characteristics in the agonist synergy shape, such as triggering times and intensity.

Thus, we have evidenced the potential of synergies in a forward dynamics pipeline and as a solution to motion control. Moreover, this work also shows that a reduced set of control signals, which is not only less than the number of actuators [20], but also less than the number of degrees of freedom, can be used to control an overactuated model, providing a promising way to command such characters for animation purposes.

## Acknowledgements

The authors wish to thank Anthony Sorel and Antoine Muller for their precious work. This study was funded by the ANR project ENTRACTE (Grant agreement: ANR 13-CORD-

002-01) [2].

# References

[1] T. Geijtenbeek and N. Pronost. Interactive character animation using simulated physics: A state-of-the-art review. *Comput. Graph. Forum*, 31(8):2492–2515, December 2012.

[2] A.L. Cruz Ruiz, C. Pontonnier, N. Pronost, and G. Dumont. Muscle-based control for character animation. *Computer Graphics Forum*, Online, 2016.

[3] J.K. Hodgins and W.L. Wooten. Animating human athletes. In *Robotics Research*, pages 356–367. Springer London, 1998.

[4] KangKang Yin, Kevin Loken, and Michiel van de Panne. Simbicon: Simple biped locomotion control. *ACM Trans. Graph.*, 26(3), July 2007.

[5] Francis Laclé and Nicolas Pronost. A scalable geometrical model for musculotendon units. *Computer Animation and Virtual Worlds*, pages n/a–n/a, 2015.

[6] A.˜V. Hill. The Heat of Shortening and the Dynamic Constants of Muscle. *Royal Society of London Proceedings Series B*, 126:136–195, 1938.

[2] ANR ENTRACTE: http://homepages.laas.fr/nmansard/entracte/index.php?n=Main.HomePage

[7] Taku Komura, Yoshihisa Shinagawa, and Tosiyasu L Kunii. Creating and retargetting motion by the musculoskeletal human body model. *The Visual Computer*, 16(5):254–270, 2000.

[8] Jack M. Wang, Samuel R. Hamner, Scott L. Delp, and Vladlen Koltun. Optimizing locomotion controllers using biologically-based actuators and objectives. *ACM Trans. Graph.*, 31(4):25:1–25:11, July 2012.

[9] Marjolein M van der Krogt, Wendy W de Graaf, Claire T Farley, Chet T Moritz, LJ Richard Casius, and Maarten F Bobbert. Robust passive dynamics of the musculoskeletal system compensate for unexpected surface changes during human hopping. *Journal of Applied Physiology*, 107(3):801–808, 2009.

[10] James C. Houk and W. Zev Rymer. *Neural Control of Muscle Length and Tension*. John Wiley & Sons, Inc., 2011.

[11] KG Gerritsen, AJ van den Bogert, M Hulliger, and RF Zernicke. Intrinsic muscle properties facilitate locomotor control-a computer simulation study. *Motor control*, 2(3):206–220, 1998.

[12] Arthur J van Soest and Maarten F Bobbert. The contribution of muscle properties in the control of explosive movements. *Biological cybernetics*, 69(3):195–204, 1993.

[13] H. Geyer and H. Herr. A muscle-reflex model that encodes principles of legged mechanics produces human walking dynamics and muscle activities. *IEEE Transactions on Neural Systems and Rehabilitation Engineering*, 18(3):263–273, June 2010.

[14] Hartmut Geyer, Andre Seyfarth, and Reinhard Blickhan. Positive force feedback in bouncing gaits? *Proceedings of the Royal Society of London B: Biological Sciences*, 270(1529):2173–2183, 2003.

[15] Arthur Prochazka, Deborah Gillard, and David J Bennett. Positive force feedback control of muscles. *Journal of Neurophysiology*, 77(6):3226–3236, 1997.

[16] Yoonsang Lee, Moon Seok Park, Taesoo Kwon, and Jehee Lee. Locomotion control for many-muscle humanoids. *ACM Trans. Graph.*, 33(6):218:1–218:11, November 2014.

[17] Ahmet Erdemir, Scott McLean, Walter Herzog, and Antonie J van den Bogert. Model-based estimation of muscle forces exerted during movements. *Clinical Biomechanics*, 22(2):131–154, 2007.

[18] Ana Lucia Cruz Ruiz, Charles Pontonnier, and Georges Dumont. A bio-inspired limb controller for avatar animation. *Computer methods in biomechanics and biomedical engineering*, 17(sup1):174–175, 2014.

[19] Nikolaj A Bernstein. The co-ordination and regulation of movements. 1967.

[20] Ana Lucia Cruz Ruiz, Charles Pontonnier, Jonathan Levy, and Georges Dumont. Motion control via muscle synergies: Application to throwing. In *Proceedings of the 8th ACM SIGGRAPH Conference on Motion in Games*, MIG '15, pages 65–72. ACM, 2015.

[21] Thomas Geijtenbeek, Michiel van de Panne, and A. Frank van der Stappen. Flexible muscle-based locomotion for bipedal creatures. *ACM Trans. Graph.*, 32(6):206:1–206:11, November 2013.

[22] Weiguang Si, Sung-Hee Lee, Eftychios Sifakis, and Demetri Terzopoulos. Realistic biomechanical simulation and control of human swimming. *ACM Trans. Graph.*, 34(1):10:1–10:15, December 2014.

[23] Igor Mordatch, Jack M. Wang, Emanuel Todorov, and Vladlen Koltun. Animating human lower limbs using contact-invariant optimization. *ACM Trans. Graph.*, 32(6):203:1–203:8, November 2013.

[24] Alla Safonova, Jessica K. Hodgins, and Nancy S. Pollard. Synthesizing physically realistic human motion in low-dimensional, behavior-specific spaces. *ACM Trans. Graph.*, 23(3):514–521, August 2004.

[25] Sumit Jain and C. Karen Liu. Modal-space control for articulated characters. *ACM Trans. Graph.*, 30(5):118:1–118:12, October 2011.

[26] Ahmed Shabana. *Vibration of discrete and continuous systems*. Springer, 1997.

[27] Yuting Ye and C. Karen Liu. Animating responsive characters with dynamic constraints in near-unactuated coordinates. *ACM Trans. Graph.*, 27(5):112:1–112:5, December 2008.

[28] Cristiano Alessandro, Ioannis Delis, Francesco Nori, Stefano Panzeri, and Bastien Berret. Muscle synergies in neuroscience and robotics: from input-space to task-space perspectives. *Frontiers in computational neuroscience*, 7, 2013.

[29] Andrea d'Avella and Francesco Lacquaniti. Control of reaching movements by muscle synergy combinations. *Frontiers in computational neuroscience*, 7, 2013.

[30] Lena H Ting. Dimensional reduction in sensorimotor systems: a framework for understanding muscle coordination of posture. *Progress in brain research*, 165:299–321, 2007.

[31] Ana Lucia Cruz Ruiz, Charles Pontonnier, Anthony Sorel, and Georges Dumont. Identifying representative muscle synergies in overhead football throws. *Computer Methods in Biomechanics and Biomedical Engineering*, 18(sup1):1918–1919, 2015.

[32] Hermie J Hermens, Bart Freriks, Roberto Merletti, Dick Stegeman, Joleen Blok, Günter Rau, Cathy Disselhorst-Klug, and Göran Hägg. European recommendations for surface electromyography. *Roessingh Research and Development*, 8(2):13–54, 1999.

[33] Peter Konrad. The abc of emg: A practical introduction to kinesiological electromyography. version 1.0, noraxon inc. 2005.

[34] Nienke W Willigenburg, Andreas Daffertshofer, Idsart Kingma, and Jaap H van Dieën. Removing ecg contamination from emg recordings: A comparison of ica-based and other filtering procedures. *Journal of electromyography and kinesiology*, 22(3):485–493, 2012.

[35] Matthew C. Tresch, Vincent C. K. Cheung, and Andrea d'Avella. Matrix factorization algorithms for the identification of muscle synergies: Evaluation on simulated and experimental data sets. *Journal of Neurophysiology*, 95(4):2199–2212, 2006.

[36] Hyunsoo Kim and Haesun Park. Nonnegative matrix factorization based on alternating nonnegativity constrained least squares and active set method. *SIAM Journal on Matrix Analysis and Applications*, 30(2):713–730, 2008.

[37] Antoine Muller, Charles Pontonnier, C Germain, and Georges Dumont. Dealing with modularity of multibody models. *Computer methods in biomechanics and biomedical engineering*, page 2, 2015.

[38] Mark De Zee, Lone Hansen, Christian Wong, John Rasmussen, and Erik B Simonsen. A generic detailed rigid-body lumbar spine model. *Journal of biomechanics*, 40(6):1219–1227, 2007.

[39] MD Klein Horsman, HFJM Koopman, FCT Van der Helm, L Poliacu Prosé, and HEJ Veeger. Morphological muscle and joint parameters for musculoskeletal modelling of the lower extremity. *Clinical biomechanics*, 22(2):239–247, 2007.

[40] Katherine RS Holzbaur, Wendy M Murray, and Scott L Delp. A model of the upper extremity for simulating musculoskeletal surgery and analyzing neuromuscular control. *Annals of biomedical engineering*, 33(6):829–840, 2005.

[41] Michael Damsgaard, John Rasmussen, Søren Tørholm Christensen, Egidijus Surma, and Mark De Zee. Analysis of musculoskeletal systems in the anybody modeling system. *Simulation Modelling Practice and Theory*, 14(8):1100–1111, 2006.

[42] Anybody managed repository. http://anyscript.org/. Accessed: 2014-09-30.

[43] Antoine Muller, Coralie Germain, Charles Pontonnier, and Georges Dumont. A simple method to calibrate kinematical invariants: Application to overhead throwing. In *33rd International Conference on Biomechanics in Sports (ISBS 2015)*, 2015.

[44] R Dumas, L Cheze, and J-P Verriest. Adjustments to mcconville et al. and young et al. body segment inertial parameters. *Journal of biomechanics*, 40(3):543–553, 2007.

[45] Carlos Rengifo, Yannick Aoustin, Franck Plestan, and Christine Chevallereau. Distribution of forces between synergistics and antagonistics muscles using an optimization criterion depending on muscle contraction behavior. *Journal of biomechanical engineering*, 132(4), 2010.

[46] Thomas S. Buchanan, David G. Loyd, Kurt Manal, and Thor F. Besier. Neuromusculoskeletal modeling : Estimation of muscle forces and joints moments and movements from measurements of neural command. *Journal of Applied Biomechanics*, 20:367–395, 2004.

[47] G. Venture, K. Yamane, and Y. Nakamura. Identifying musculo-tendon parameters of human body based on the musculo-skeletal dynamics computation and hill-stroeve muscle model. In *2005 5th IEEE-RAS International Conference on Humanoid Robots*, pages 351–356, Dec 2005.

[48] G Venture, K Yamane, and Y Nakamura. Application of non-linear least square method to estimate the muscle dynamics of the elbow joint. In *IFAC - Int. Conf. on System Identification*, pages 1168–1173, Newcastle, Australia, 2006.

[49] JB Lee, T Matsumoto, T Othman, M Yamauchi, A Taimura, E Kaneda, N Ohwatari, and M Kosaka. Coactivation of the flexor muscles as a synergist with the extensors during ballistic finger extension movement in trained kendo and karate athletes. *International journal of sports medicine*, 20(1):7–11, January 1999.

[50] Masaya Hirashima, Hiroshi Kadota, Shizuka Sakurai, Katzutoshi Kudo, and Tatsuyuki Ohtsuki. Sequential muscle activity and its functional role in the upper extremity and trunk during overarm throwing. *Journal of Sports Sciences*, 20(4):301–310, 2002.

[51] S. Sakurai and T. Ohtsuki. Muscle activity and accuracy of performance of the smash stroke in badminton with reference to skill and practice. *Journal of Sports Sciences*, 18(11):901–914, 2000.

[52] Joo H Kim, Yujiang Xiang, Jingzhou Yang, Jasbir S Arora, and Karim Abdel-Malek. Dynamic motion planning of overarm throw for a biped human multibody system. *Multibody System Dynamics*, 24(1):1–24, 2010.

# Appendix A

## Details on data acquisition and processing

Motion was captured with a Vicon system (15 cameras, 100Hz sampling rate). The joints coordinates were estimated from the motion capture data, with an inverse kinematics method allowing the segment lengths and marker positions to be calibrated [43].

The muscle activity was collected using surface electrodes (Cometa Waveplus EMG system, 1000Hz sampling rate) and well known electrode placement standards [32]. The collected EMG signals were then processed by following well known processing protocols [33]. These signals were amplified (gain 1000), digitized (1kHz), band-pass filtered (10-450Hz), rectified, and low-pass filtered (6Hz). ECG artifacts were removed using an ICA-based filtering procedure [34].

# Appendix B

## Skeletal model

The full body skeletal model consists of 21 rigid bodies linked by 17 joints, and exhibits 32 degrees of freedom. The method used to describe the skeletal model is based on a systematic structural representation. Except for the root (pelvis), each segment integrates a joint and its adjoined body. Thus, the segment representation does not depend on the other segments connected to it. This structural representation is described according to a hierarchical tree. From the root, each solid owns one child and one sister. A library containing several body part models issued from the literature, which can correspond to a segment or a set of segments, was used to build the model [37]. The model used in the current study consists of well known and validated biomechanical models of the spine [38], the lower limbs [39] and the upper limbs [40]. The complete skeletal model has been kinematically validated [43]. Furthermore, the bone graphics were adapted from the AnyBody Managed Repository [41, 42].

Standard Body Segment Inertial Parameters (BSIP) were estimated using an anthropometric scaling rule to adapt the model to the subject's morphology [44].

## Musculotendon unit model

Section *Musculoskeletal arm model*, featured a brief explanation of the geometric and functional model used for the musculotendon units. Here we explain such models in detail. Geometrically, the muscles are pulley-like, and thus their insertion points are not explicitly defined, instead a joint rest position $qr_k$ and a rest musculotendon length $l_{mtr,j}$ are specified.

The total length of the unit $l_{mt,j}$ can be expressed as:

$$l_{mt,j} = l_{mtr,j} - r_{j,k}(q_k - qr_k) \tag{10}$$

or as the sum of the muscle length $l_{m,j}$ and the constant tendon length $l_{t,j}$ (infinitely rigid tendon):

$$l_{mt,j} = l_{m,j} + l_{t,j} \tag{11}$$

By solving equation 11 for $l_{m,j}$ and replacing $l_{mt,j}$ from equation 10, the changes in muscle length $l_{m,j}$ and shortening velocity $\dot{l_{m,j}}$ can be described as follows:

$$l_{m,j} = l_{mtr,j} - r_{j,k}(q_k - qr_k) - l_{t,j} \tag{12}$$

$$\dot{l_{m,j}} = -r_{j,k}\dot{q_k} \tag{13}$$

The functional model used for the musculotendon unit consisted of a Hill muscle model [6]. As shown in figure 13, this model consists of a contractile element $CE$ (non-linear visco-elastic relationship) in parallel with a passive element $PE$ (non-linear spring), and in

series with a tendon $SE$ (serial non-linear spring). It is also characterized by a pennation angle $\alpha$, representing the orientation of the fibers with regard to the tendon. This model has been widely used in biomechanics, and recently within the animation community [23, 8], even if the numerous parameters necessary to completely define its behavior are difficult to obtain in vivo.

With this model, the muscle force $F_{m,j}$ of a musculotendon unit $j$ can be summarized as the sum of the contractile and passive forces:

$$F_{m,j} = [f_p(\bar{l}_{m,j}) + a_j \cdot f_l(\bar{l}_{m,j}) \cdot f_v(\dot{\bar{l}}_{m,j})] \cdot F_{o,j} \tag{14}$$

Where $f_p$ is the passive force relationship, $a_j$ is the muscle activation, $f_l$ is the force-length relationship, $f_v$ the force-velocity relationship, $F_{o,j}$ is the maximum isometric force, and $\bar{l}_{mj}$ the normalized length of the muscle unit. This length is obtained by dividing the muscle length by its optimal fiber length $l_{o,j}$.

Several models have been proposed to approximate the $f_l$, $f_v$ and $f_p$ relationships with regard to experimental data. The chosen models for this work are featured in Figure 14 [45].

Once the muscle force has been determined, the force at the tendon $f_{t,j}$ can be obtained by simply taking into account the pennation angle of the fibers:

$$f_{t,j} = F_{m,j} \cdot \cos \alpha_j \tag{15}$$

In this study the pennation angle was neglected, and therefore $F_{m,j}$ was directly the output of the musculotendon unit.

# Appendix C

## Combination coefficients filter

The filter which was applied to the optimized combination coefficients is detailed in this section. After expressing the activations dynamics in the Laplace domain (equation 9), its z-transform can be written as:

$$\frac{c_i(z)}{c_{iraw}(z)} = \frac{b_1 z + b_0}{a_2 z^2 + a_1 z + a_0} \tag{16}$$

With

$b_1 = \frac{\tau_{ne}(1-e^{-T_e/\tau_{ne}})-\tau_{act}(1-e^{-T_e/\tau_{act}})}{\tau_{ne}-\tau_{act}}$

$b_0 = e^{-T_e/\tau_{ne}} e^{-T_e/\tau_{act}} - \frac{e^{-T_e/\tau_{ne}}-e^{-T_e/\tau_{act}}}{\tau_{act}-\tau_{ne}}$

$a_2 = 1$

$a_1 = -(e^{-T_e/\tau_{ne}} + e^{-T_e/\tau_{act}})$

$a_0 = e^{-T_e/\tau_{ne}} e^{-T_e/\tau_{act}}$

Equation 16 can then be multiplied by $z^{-2}$ to be only dependent of negative powers of z, and finally, thanks to the delay theorem, we can write the following recursive equation:

$$\begin{aligned} c_i(hT_e) &= -a_1 c_i((h-1)T_e) - a_0 c_i((h-2)T_e) \\ &\quad + b_1 c_{iraw}((h-1)T_e) + b_0 c_{iraw}((h-2)T_e) \end{aligned} \tag{17}$$

Where $T_e$ is the sampling time, $0.01s$ in our case. The sampling resulted in a static gain equal to $H = \frac{(b_1+b_0)}{(a_2+a_1+a_0)}$, therefore equation 18 was divided by this gain to get a normalized

combination coefficient:

$$c_{i_{norm}}(hT_e) = \frac{c_i(hT_e)}{H} \tag{18}$$

# Biographies

Ana Lucia Cruz Ruiz is a Ph.D candidate in the INRIA/IRISA MimeTic research team and at the École Normale Supérieure de Rennes since 2013. She received her M.Sc degree in robotics and control from École Centrale de Nantes, France in 2013. Her research focuses on the design of original bio-inspired controllers for virtual character motion synthesis.

Charles Pontonnier received his PhD degree in mechanics in 2010 from Rennes 1 University. He is associate professor at École Normale Supérieure de Rennes on secondment at military academy of Saint-Cyr Coëtquidan since 2012. His current research focuses on muscle-based motion analysis-synthesis for ergonomics and virtual reality tools for ergonomics.

Jonathan Lévy is a student of department in Mechatronics of Ecole normale supérieure de Rennes, France. He is in first year of Master's degree in mechanical engineering from Rennes 1 university and Ecole normale supérieure de Rennes, France, and in first year of Master's degree of electronics and telecommunication from Rennes 1 university, France.

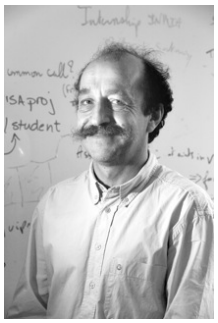

Georges Dumont is a Professor in Mechanical Sciences at École Normale Supérieure de Rennes in Rennes, France. He received his PhD in computer science from Rennes 1 University in 1990 and his habilitation in mechanical science in 2005. His main research interests include physical simulation, mechanics, biomechanics, haptic rendering, interactive collaboration and virtual reality.

# Illustrations

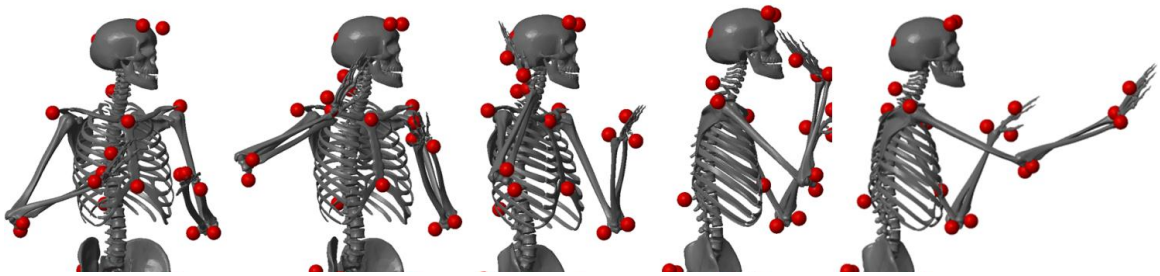

Figure 1: Overhead throw to 2m target

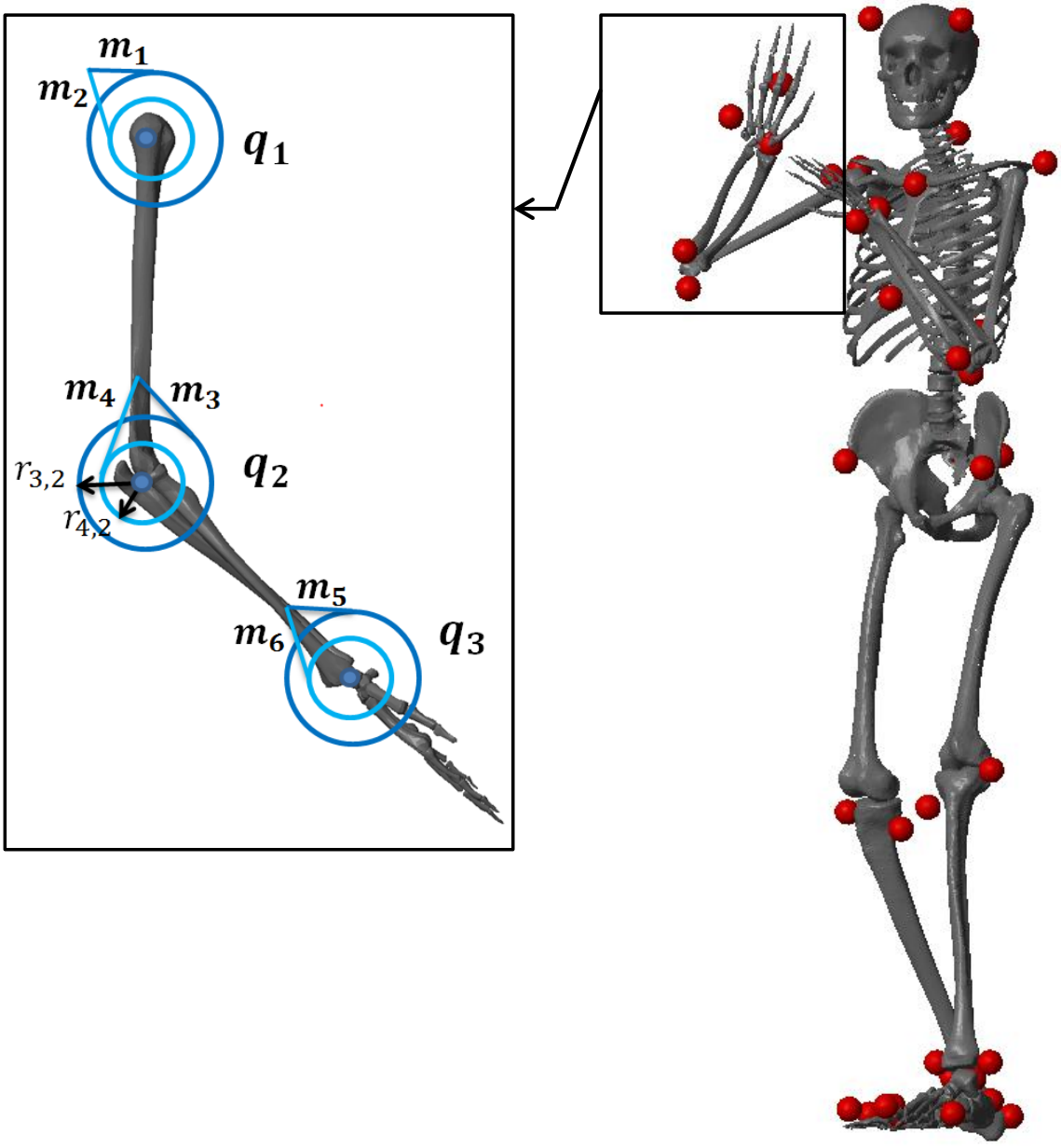


Figure 2: Full body skeletal model and musculoskeletal arm model

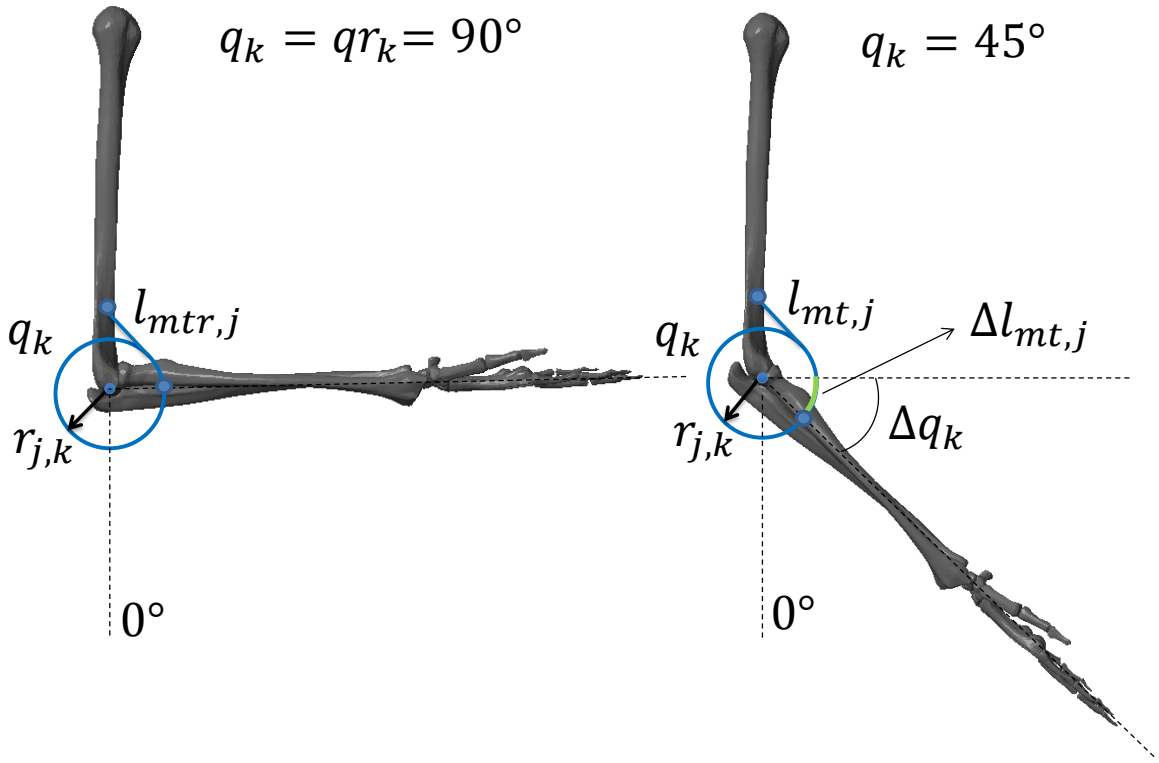


Figure 3: Musculotendon geometric model

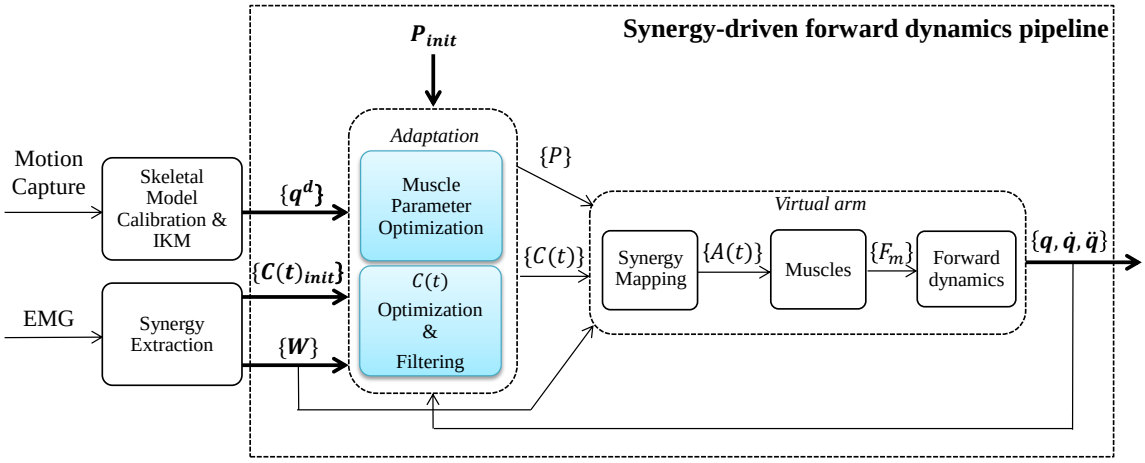


Figure 4: Synergy-driven forward dynamics pipeline

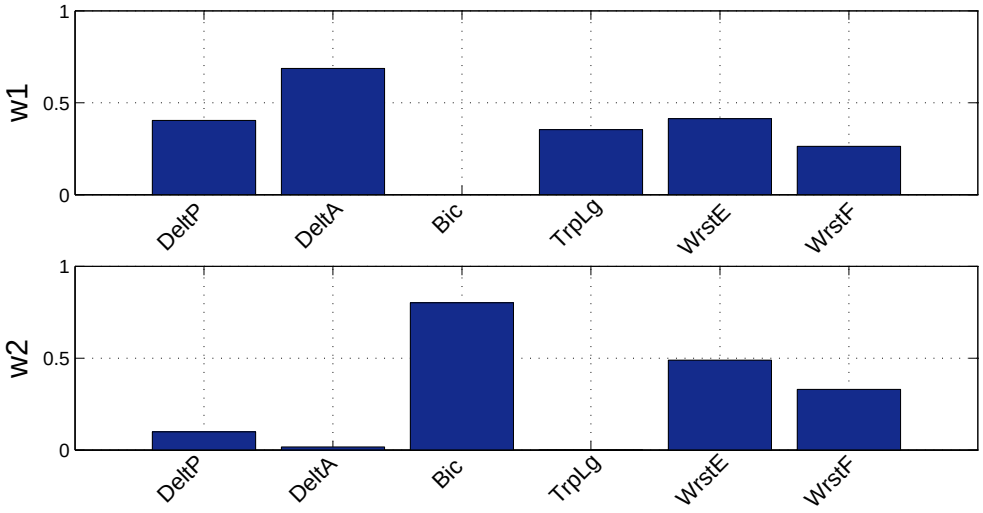


Figure 5: Extracted synergies $w_i$

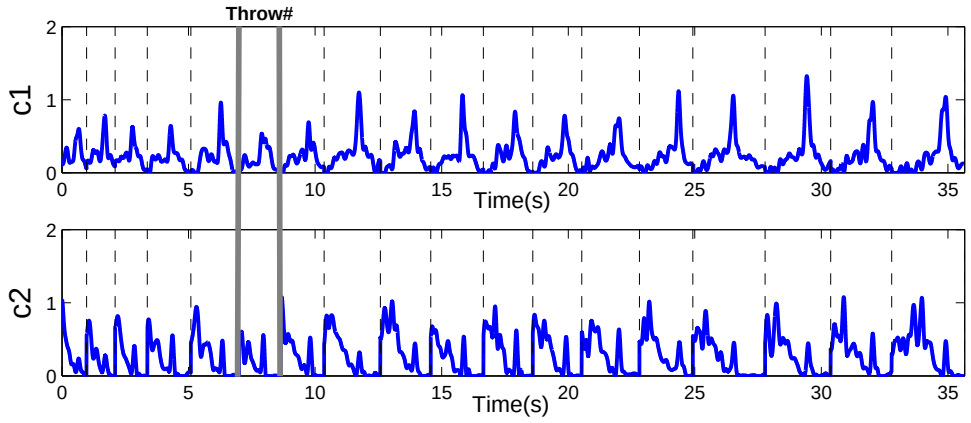


Figure 6: Extracted time-varying combination coefficients $c_i$

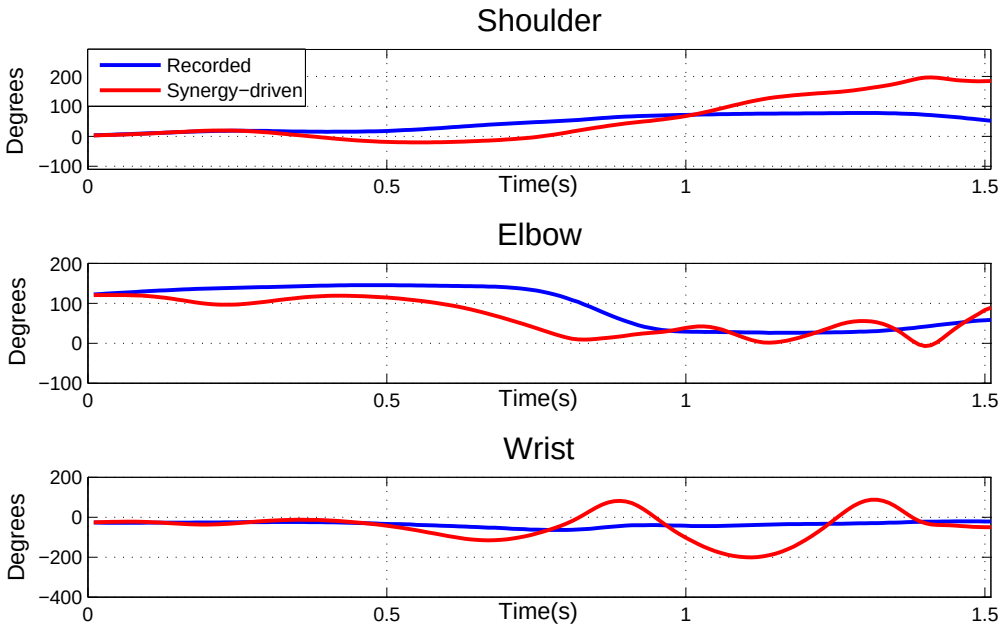


Figure 7: Synergy-driven motion with uncertain muscle parameters

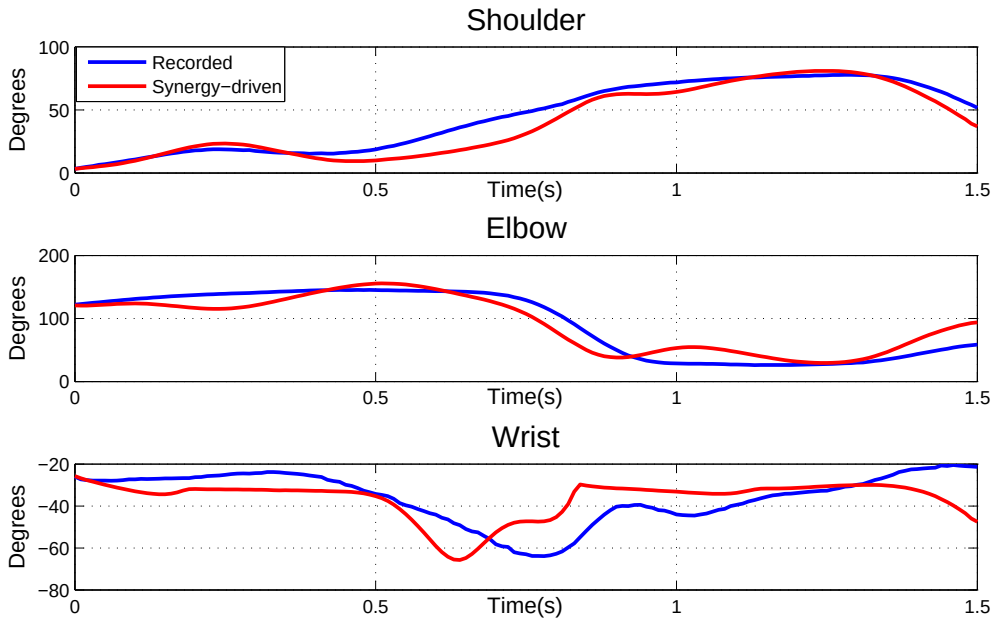


Figure 8: Synergy-driven motion with optimized muscle parameters

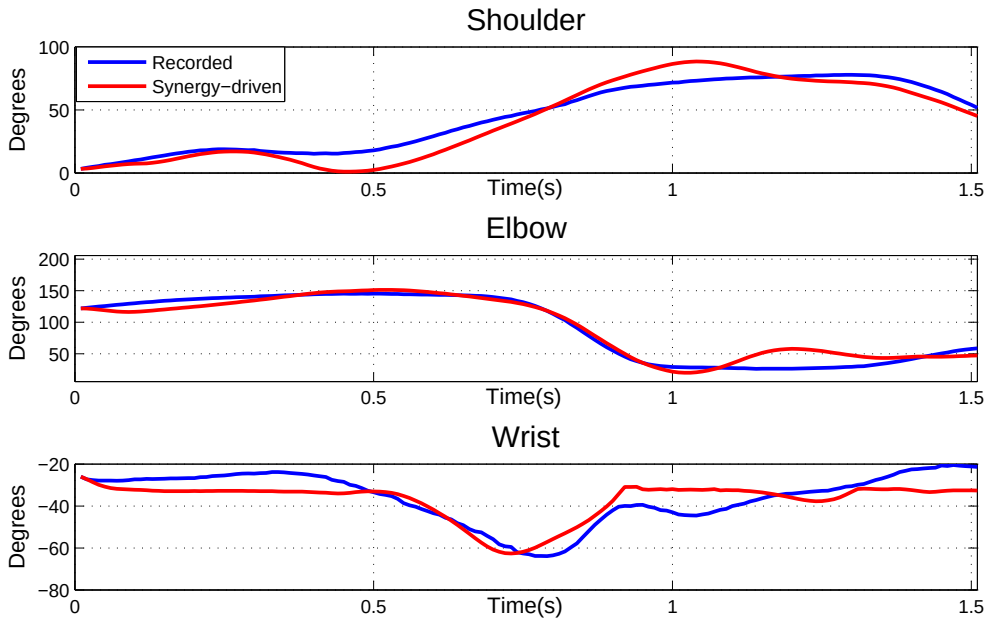


Figure 9: Motion after $C(t)$ optimization and filtering

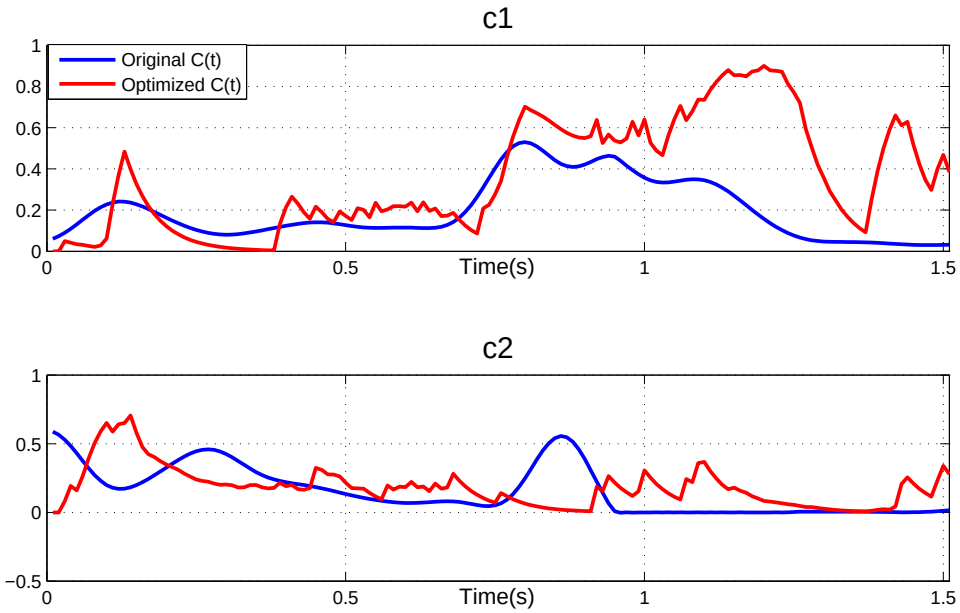


Figure 10: $C(t)$ before and after optimization and filtering

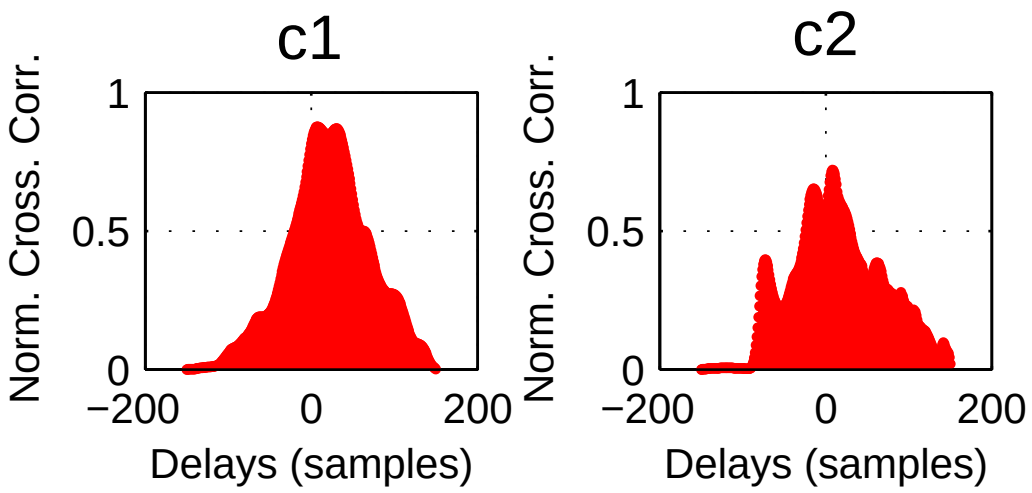


Figure 11: Cross-correlation between the original and optimized $C(t)$ for the 2-synergy model

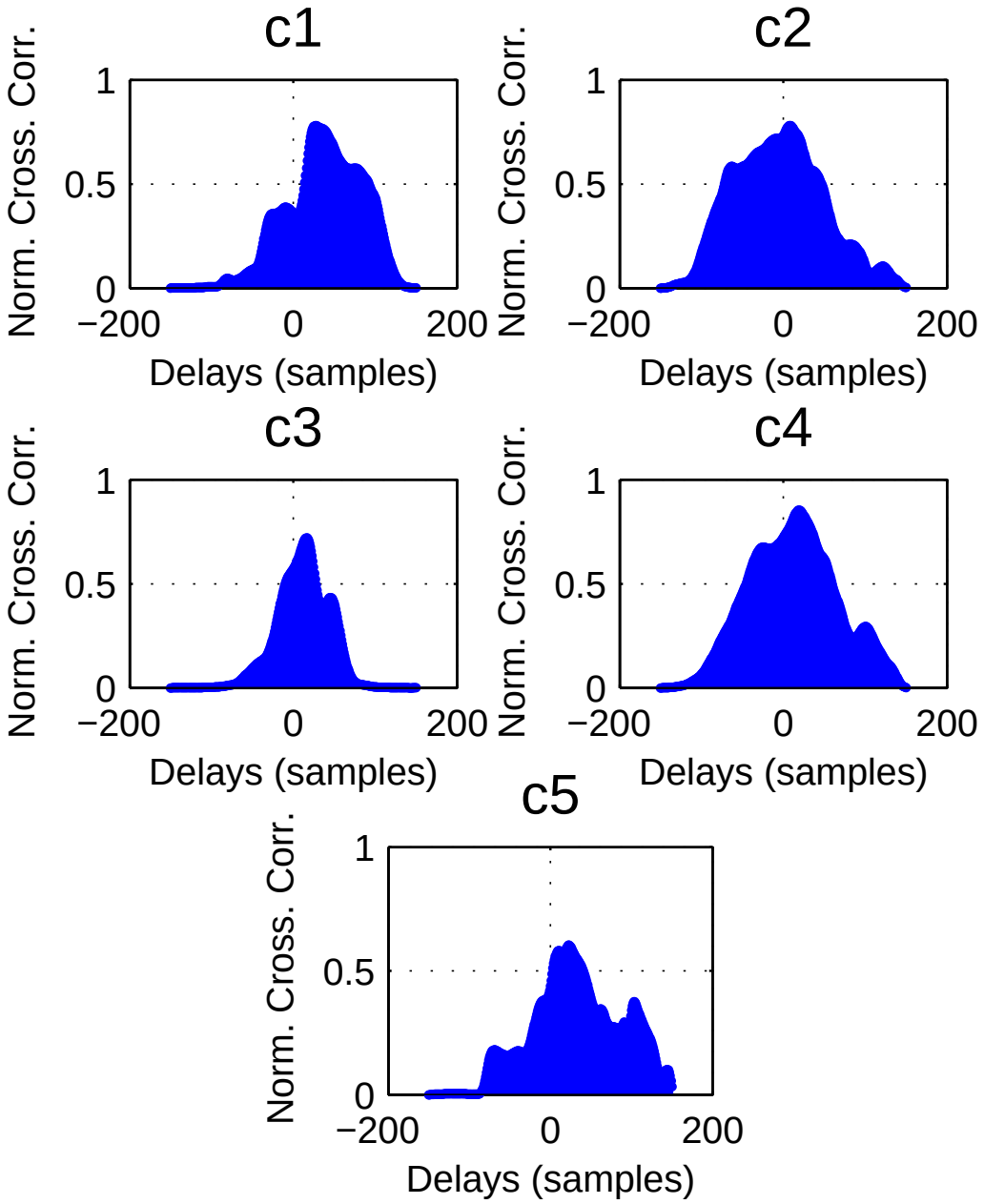


Figure 12: Cross-correlation between the original and optimized $C(t)$ for the 5-synergy model

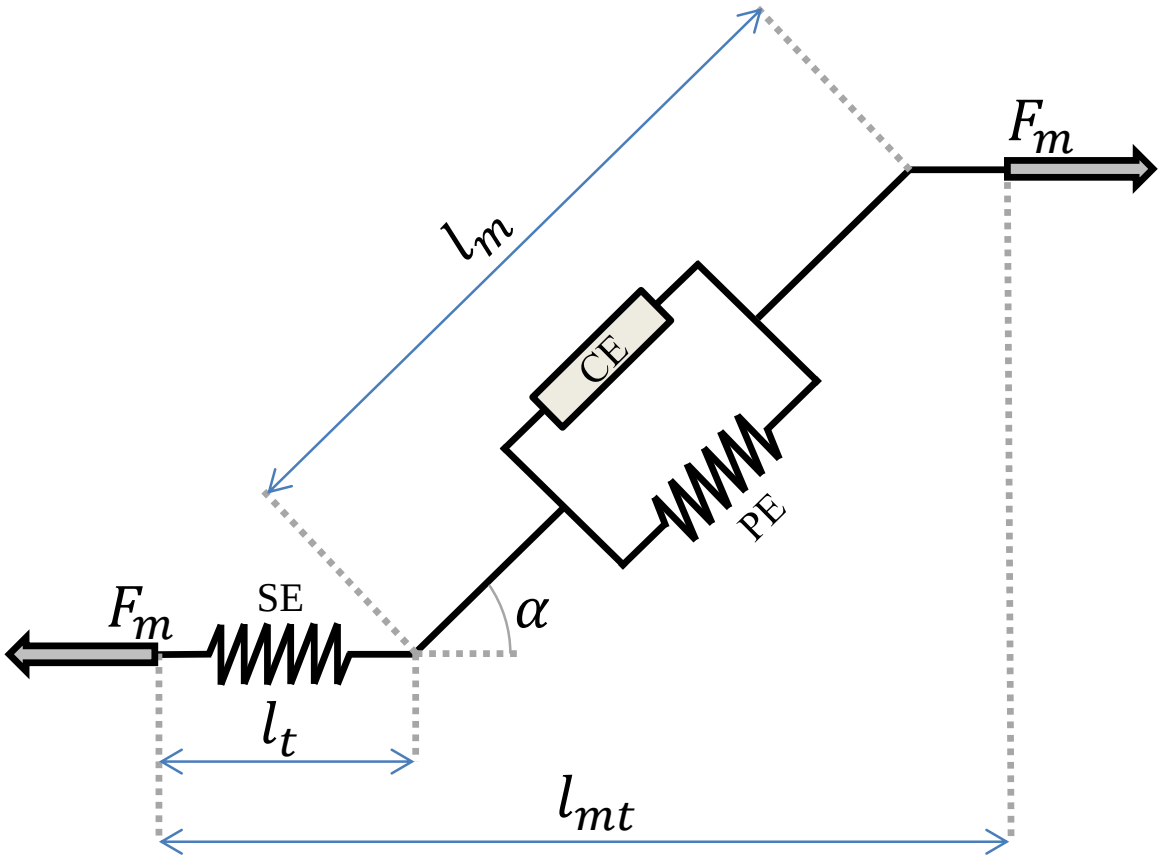


Figure 13: Musculotendon functional model adapted from [17]

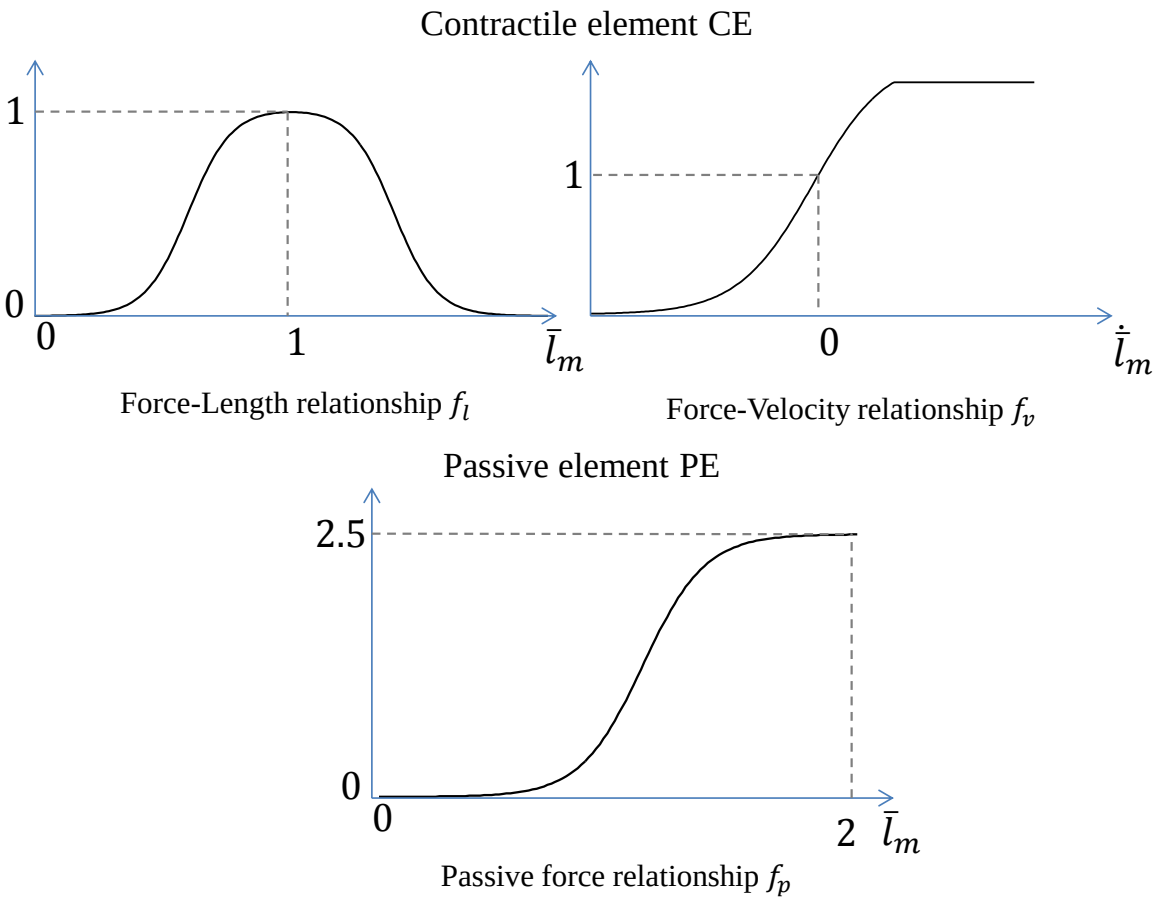


Figure 14: Force generation capacity of muscles

| Coefficient of determination ($r^2$) | | | |
|---|---|---|---|
| Synergy model | Shoulder | Elbow | Wrist |
| 2-synergy model | 0.8939 | 0.8843 | 0.2732 |
| 5-synergy model | 0.8971 | 0.8904 | negative |

Table 1: Quality of motion reconstruction after muscle parameter optimization

| Coefficient of determination ($r^2$) | | | |
|---|---|---|---|
| Synergy model | Shoulder | Elbow | Wrist |
| 2-synergy model | 0.8859 | 0.9489 | 0.6746 |
| 5-synergy model | 0.9268 | 0.9420 | 0.8136 |

Table 2: Quality of motion reconstruction after $C(t)$ optimization and filtering